THE 'HALO' FAMILY OF 3-DIMENSIONAL PERIODIC ORBITS IN THE EARTH–MOON RESTRICTED 3-BODY PROBLEM

JOHN V. BREAKWELL

Department of Aeronautics/Astronautics, Stanford University, 94305, U.S.A.

JOHN V. BROWN

*Western Development Lab. Division, Ford Aerospace and Communication Corp.,
Palo Alto, Calif., U.S.A.*

Abstract. The Halo orbits originating in the vicinities of both L_1 and L_2 grow larger, but shorter in period, as they shift towards the Moon. There is in each case a narrow band of stable orbits roughly half-way to the Moon. Nearer to the Moon, the orbits are fairly well-approximated by an 'almost rectilinear' analysis. The L_2 family shrinks in size as it approaches the Moon, becoming stable again shortly before penetrating the lunar surface. The L_1-family becomes longer and thinner as it approaches the Moon, with a second narrow band of stable orbits with perilune, however, below the lunar surface.

1. Introduction

Farquhar and Kamel [1] computed a family of 'halo' orbits near the translunar L_2 libration point but permanently 'visible' from Earth.

The existence of such orbits had been suspected for reasons set forth in the following two paragraphs:

The linearized motion near L_2, although unstable, includes a periodic motion in the xy plane, i.e., in the plane of the relative Earth–Moon motion, of frequency $1.86n$, where n is the angular rate of the Moon and the Earth. The instability manifests itself by real additional characteristic roots $\pm 2.16n$. The out-of-plane linearized z-motion is simple harmonic with frequency $1.79n$. If, as pointed out by Farquhar [2], initial conditions were to produce a periodic xy-motion and a z-motion, with phase initially 90° ahead or behind that of the xy-motion, the resulting orbit could remain continuously visible from Earth for many months, before the relative phase approaches 0 or 180°, thereby producing periodic occultation by the Moon.

If an orbit, however, is of a size comparable with the distance of L_2 from the Moon, so that nonlinear terms become significant, nonlinear dependence of frequency on amplitude as well as nonlinear coupling might produce a purely periodic three-dimensional motion.

Farquhar and Kamel computed these orbits by a truncated Linstedt-Poincaré series. This series included, moreover, quasi-periodic additions due to solar gravity and lunar orbital eccentricity, which effects will naturally be ignored in this paper. Projections of typical periodic orbits obtained by the truncated series are shown in
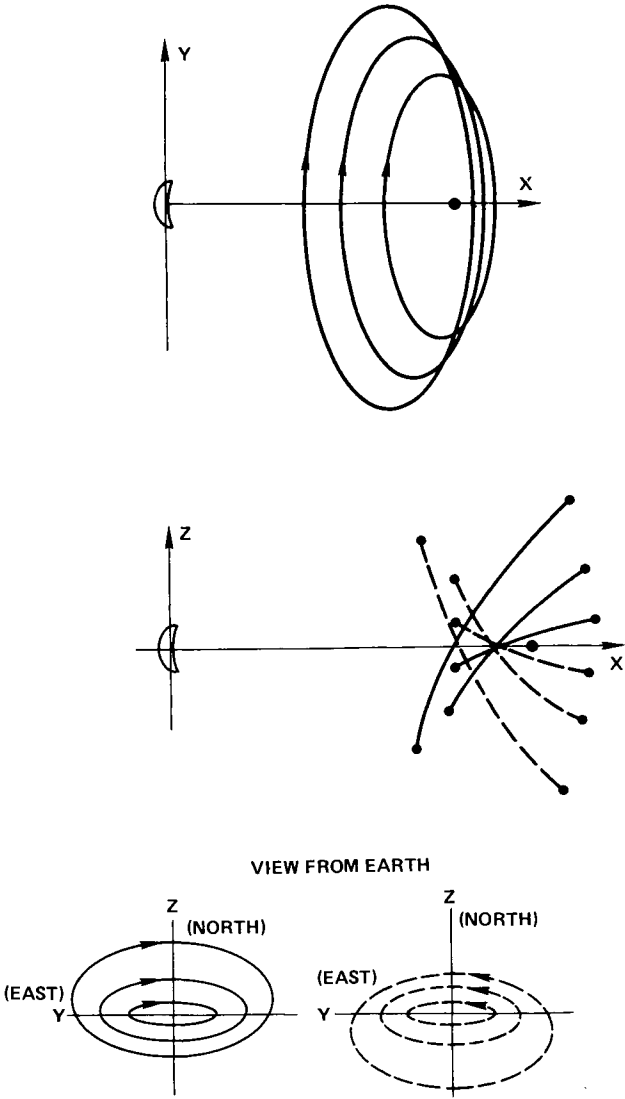
Fig. 1.   Halo orbits near L_2.

Figure 1. The solid lines show the northern halo family for which z is in phase with x and 90° behind y; the dotted lines show the mirror-image southern family obtained by reversing the sign of z. The convergence of the series deteriorates for orbits larger than those shown.

2. Analysis

If position is measured in the usual rotating frame with origin at the Earth–Moon barycenter, and if units of time and distance are chosen so that $n = 1$ and Earth–

Moon distance $= 1$, the equations of motion are

$$\ddot{x} - 2\dot{y} = \frac{\partial U}{\partial x}$$

$$\ddot{y} + 2\dot{x} = \frac{\partial U}{\partial y} \qquad (2.1)$$

$$\ddot{z} = \frac{\partial U}{\partial z}$$

where

$$U(x, y, z) = \tfrac{1}{2}(x^2 + y^2) + \frac{1 - \mu}{d_\oplus(x, y, z)} + \frac{\mu}{d_\text{\Moon}(x, y, z)}, \qquad (2.2)$$

$\mu/(1 - \mu)$ being the Moon–Earth mass-ratio, and $d_\oplus$ and $d_\text{\Moon}$ denoting distances from Earth and Moon respectively.

A 1-parameter extension of the Farquhar–Kamel family of halo orbits is obtained by adjusting values of x_0, z_0, $\dot{y}_0$ at a perpendicular crossing of the xz plane (i.e., $y_0 = \dot{x} = \dot{z}_0 = 0$), so that the next crossing of this plane, $y_1 = 0$ at $t = t_1$, sgn $\dot{y}_1 = -\text{sgn}\ \dot{y}_0$ is also perpendicular; i.e., the velocity components $\dot{x}_1$ and $\dot{z}_1$ are also zero. Because of the invariance of Equations (2.1) under the reflection $t \to -t$, $y \to -y$, it follows that such an orbit will necessarily repeat with period $T = 2t_1$. It will suffice to investigate the northern halo family.

The 6×6 transition-matrix $\Phi(t, 0)$ associated with (2.1) is the matrix of partial derivatives $\partial X(t)/\partial X(0)$, where X denotes a column-vector with entries x, y, z, $\dot{x}$, $\dot{y}$, $\dot{z}$. $\Phi(t, 0)$ satisfies, of course, the matrix differential equation and initial condition:

$$\frac{\mathrm{d}}{\mathrm{d}t} \Phi(t, 0) = F(t)\Phi(t, 0), \ \Phi(0, 0) = \text{identity matrix}, \qquad (2.3)$$

where

$$F(t) = \left(-\frac{0}{U_{XX}} \bigg| \frac{I}{2\Omega} \right), \qquad (2.4)$$

in which I denotes the 3×3 identity matrix,

$$\Omega = \begin{pmatrix} 0 & 1 & 0 \\ -1 & 0 & 0 \\ 0 & 0 & 0 \end{pmatrix}, \qquad (2.5)$$

and $U_{XX}(t)$ denotes the symmetric matrix of second partial derivatives of U w.r.t. x, y, z, evaluated along the orbit.

The transition-matrix $\Phi(t_1, 0)$ at the end of a half-cycle of a nearly periodic orbit can be used to adjust the initial conditions so as to obtain periodicity. For example, if

x_0 is held fixed,

$$\begin{pmatrix} \delta \dot{x}_1 \\ \delta \dot{z}_1 \end{pmatrix} = \begin{pmatrix} \Phi_{43} & \Phi_{45} \\ \Phi_{63} & \Phi_{65} \end{pmatrix} \begin{pmatrix} \delta \dot{z}_0 \\ \delta \dot{y}_0 \end{pmatrix} + \begin{pmatrix} \ddot{x}_1 \\ \ddot{z}_1 \end{pmatrix} \delta t,$$

where

$$0 = \delta y_1 = (\Phi_{23} \quad \Phi_{25}) \begin{pmatrix} \delta z_0 \\ \delta \dot{y}_0 \end{pmatrix} + \dot{y}_1 \delta t,$$

and where Φ_{ij} is a typical element of $\Phi(t_1, 0)$. Hence

$$\begin{pmatrix} \delta \dot{x}_1 \\ \delta \dot{z}_1 \end{pmatrix} = \left[\begin{pmatrix} \Phi_{43} & \Phi_{45} \\ \Phi_{63} & \Phi_{65} \end{pmatrix} - \frac{1}{\dot{y}_1} \begin{pmatrix} \ddot{x}_1 \\ \ddot{z}_1 \end{pmatrix} (\Phi_{23} \quad \Phi_{25}) \right] \begin{pmatrix} \delta z_0 \\ \delta \dot{y}_0 \end{pmatrix},$$

and a 2×2 inversion yields $\begin{pmatrix} \delta z_0 \\ \delta \dot{y}_0 \end{pmatrix}$ so that $\begin{pmatrix} \delta \dot{x}_1 \\ \delta \dot{z}_1 \end{pmatrix}$ cancels any previous $\begin{pmatrix} \dot{x}_1 \\ \dot{z}_1 \end{pmatrix}$, if sufficiently small. This provides an iterative calculation of z_0, $\dot{y}_0$.

The transition-matrix at the end of a full cycle of the periodic orbit is

$$\Phi(T, 0) = \Phi(2t_1, 0).$$

Its eigen-values determine the stability of the orbit; two of the eigen-values are always unity and the other four eigen-values form a self-reciprocal set $(\lambda_1, 1/\lambda_1, \lambda_2, 1/\lambda_2)$, as follows from the invariance of (2.1) under $t \to -t$, $y \to -y$. The periodic orbit is thus unstable unless both λ_1 and λ_2 lie on the unit-circle.

In the interest of numerical accuracy, the full-cycle transition-matrix $\Phi(2t_1, 0)$ can be obtained from the half-cycle transition-matrix $\Phi(t_1, 0)$ without the necessity of numerical integration beyond time $t = t_1$. This is possible because, if $\Phi^*(t, 0)$ denotes

$$\left(\begin{array}{c|c} I & 0 \\ \hline -\Omega & I \end{array} \right) \Phi(t, 0) \left(\begin{array}{c|c} I & 0 \\ \hline \Omega & I \end{array} \right), \quad \Phi^* \text{ is 'symplectic',}$$

i.e.,

$$\Phi^{*T} \left(\begin{array}{c|c} 0 & I \\ \hline -I & 0 \end{array} \right) \Phi^* = \left(\begin{array}{c|c} 0 & I \\ \hline -I & 0 \end{array} \right),$$

as follows rather easily from the Hamiltonian form of the equations of motion if, instead of velocity components $\dot{x}$, $\dot{y}$, $\dot{z}$, we make use of generalized momenta: $p_x = \dot{x} - y$, $p_y = \dot{y} + x$, $p_z = \dot{z}$. The symplectic property of Φ^*, together with the invariance of (2.1) under $t \to -t$, $y \to -y$, leads to:

$$\Phi(0, -t_1) = A \Phi(0, t_1) A = A \left(\begin{array}{c|c} 0 & I \\ \hline -I & 2\Omega \end{array} \right) \Phi^T(t_1, 0) \left(\begin{array}{c|c} 2\Omega & -I \\ \hline I & 0 \end{array} \right) A,$$

$$(2.6)$$

where A denotes

$$\begin{pmatrix} 1 & & & & & \\ & -1 & & & 0 & \\ & & 1 & & & \\ & & & -1 & & \\ 0 & & & & 1 & \\ & & & & & -1 \end{pmatrix}$$

Finally

$$\Phi(2t_1, 0) = \Phi(2t_1, t_1)\Phi(t_1, 0) = \Phi(0, -t_1)\Phi(t_1, 0) . \tag{2.7}$$

The four critical eigen-values $(\lambda_1, 1/\lambda_1, \lambda_2, 1/\lambda_2)$ can be obtained with greater numerical accuracy as the eigen-values of a 4×4 matrix M derivable from $\Phi(2t_1, 0)$. This derivation makes use of the well-known constancy, along any solution of (2.1), of Jacobi's constant:

$$C = 2U(x, y, z) - (\dot{x}^2 + \dot{y}^2 + \dot{z}^2) . \tag{2.8}$$

Suppose, then, that $x_0, z_0, \dot{x}_0, \dot{z}_0$ (but not y_0) are varied in such a way that C is unchanged, so that

$$\delta\dot{y}_0 = -\frac{1}{C_{\dot{y}_0}}(C_{x_0}\delta x_0 + C_{z_0}\delta z_0) , \tag{2.9}$$

where use has been made of the vanishing of the partial derivatives $C_{\dot{x}_0}$ and $C_{\dot{z}_0}$ when $\dot{x}_0 = \dot{z}_0 = 0$. Furthermore, the correction δT to the time of the second crossing of the xz plane after time zero is given by

$$dy_2 = \dot{y}(T)\delta T + (\partial y/\partial x_0, \partial y/\partial z_0, \partial y/\partial \dot{x}_0, \partial y/\partial \dot{y}_0, \partial y/\partial \dot{z}_0) \cdot$$

$$\cdot \begin{pmatrix} \delta x_0 \\ \delta z_0 \\ \delta \dot{x}_0 \\ \delta \dot{y}_0 \\ \delta \dot{z}_0 \end{pmatrix} = 0 \tag{2.10}$$

in which $\dot{y}(T) = \dot{y}_0$. It follows easily from (2.9) and (2.10) that

$$\begin{pmatrix} dx_2 \\ dz_2 \\ d\dot{x}_2 \\ d\dot{z}_2 \end{pmatrix} = M \begin{pmatrix} \delta x_0 \\ \delta z_0 \\ \delta \dot{x}_0 \\ \delta \dot{z}_0 \end{pmatrix} , \tag{2.11}$$

where

$$M = \Phi^{\ddagger} - \frac{1}{C_{\dot{y}_0}} \, \Phi^{\ddagger}_{.5}(C_{x_0}, C_{z_0}, 0, 0)$$

$$- \frac{1}{\dot{y}_0} \begin{pmatrix} 0 \\ 0 \\ \ddot{x}_0 \\ \ddot{z}_0 \end{pmatrix} \left[\Phi^{\ddagger}_{2.} - \frac{1}{C_{\dot{y}_0}} \Phi_{25}(C_{x_0}, C_{z_0}, 0, 0) \right], \qquad (2.12)$$

in which $\Phi^{\ddagger}$ denotes the result of deleting the second and fifth rows and columns of $\Phi(2t_1, 0)$, $\Phi^{\ddagger}_{.5}$ the fifth column of $\Phi(2t_1, 0)$ without rows 2 and 5, and $\Phi^{\ddagger}_{2.}$ the second row without columns 2 and 5.

3. Numerical Results

The eigen-values $(\lambda_1, 1/\lambda_1, \lambda_2, 1/\lambda_2)$ of M have been computed, along with the periodic orbits themselves, at frequent intervals of $x_0 = x_{\max}$ (now measured from the Moon, away from the Earth); the xz projections of the orbits are shown in Figure 2. The eigen-values turn out either to be real or to lie on the unit-circle. Stability is thus conveniently decided by the values of two stability indices: $\nu_i = \frac{1}{2}[\lambda_i + (1/\lambda_i)]$ $(i = 1, 2)$: the orbit is stable if both $|\nu_1|$ and $|\nu_2| < 1$, unstable if either
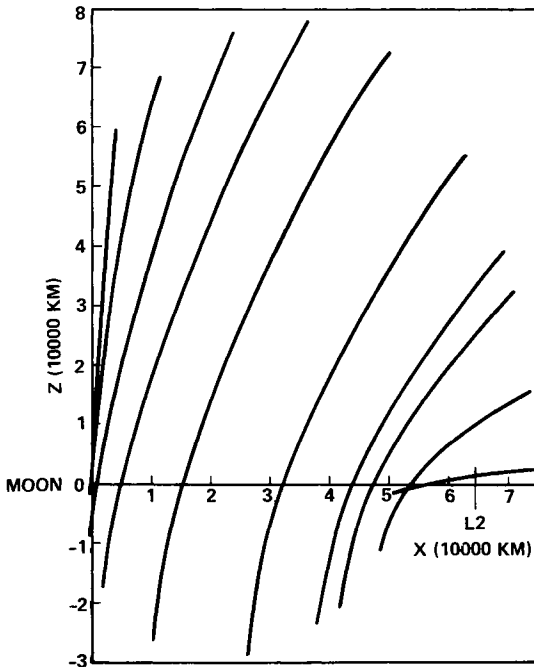

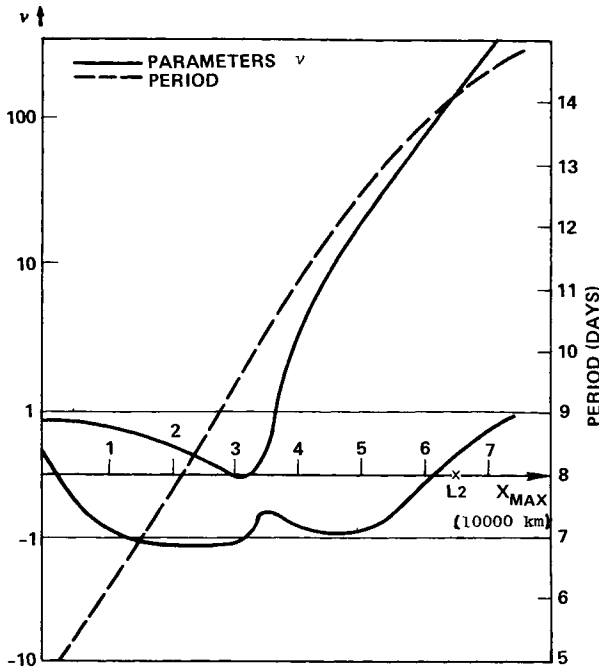Fig. 2. X–Z projection of the L_2 Halo family.

Fig. 3.   Stability parameters ν_i and period.

$|\nu_i| > 1$. The indices ν_1, ν_2 are plotted in Figure 3 vs x_{max}, along with the orbital period. The drastic instability of the family close to L_2 diminishes as the orbits grow nearer to the Moon and shorter in period. There is actually a narrow band of stable orbits for x_{max} between 36 500 km (where one pair of λ's coincides at +1 and the Jacobi constant reaches a minimum) and 31 300 km (where the other pair of λ's coincides at -1). Projections of this band of stable orbits are shown in Figures 4a–c.

The existence, but not the stability, of such orbits can be understood by regarding them as orbits of the Moon with a substantial Earth perturbation. Thus the tilt of the xz projection away from the Earth as z increases (Figure 4a) provides a torque, due to the Earth's gravity–gradient, about the positive y-axis, causing the orbital angular momentum vector $\mathbf{h}/\mathbb{C}$, relative to the Moon, to precess and keep the orbit fixed in the rotating frame.

As x_{max} decreases further, the orbits grow mildly unstable and then stable again at $x_{max} = 28\ 500$ km, $(d_{\mathbb{C}})_{min} \cong 4000$ km, and for x_{max} less than 3000 km, the maximum z is less than 64 000 km, $(d_{\mathbb{C}})_{min}$ falls below 1740 km and the orbits intersect the lunar surface.

4. The Almost Rectilinear Orbits

The almost rectilinear orbits towards which the halo family tends as x_{max} decreases are amenable to an analytical approximation used in reference [3] in a different
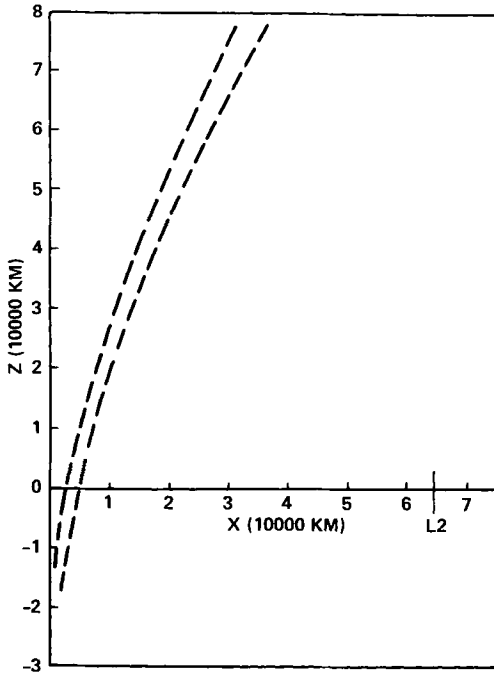
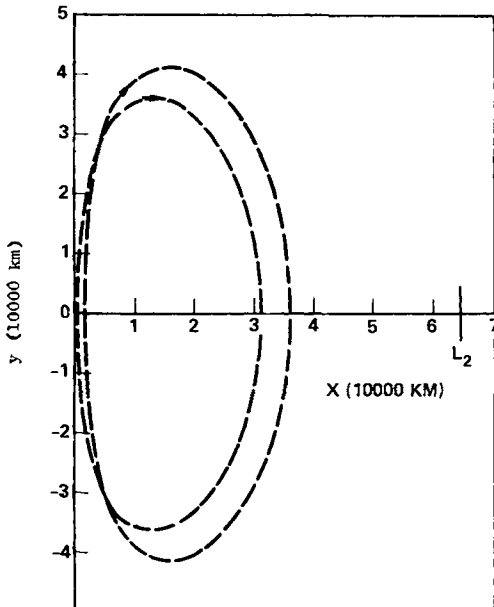Fig. 4a.   Stable orbit X–Z position bounds, L_2 branch.

Fig. 4b.   Stable orbit X–Y position bounds, L_2 branch.
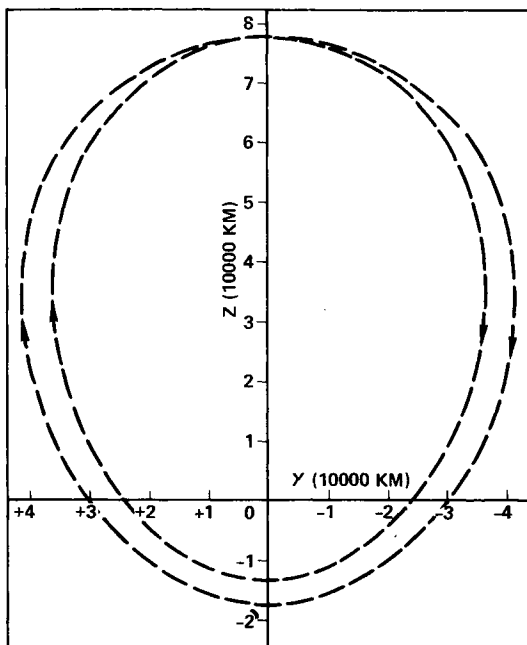
Fig. 4c.   Stable orbit Y–Z position bounds, L_2 branch.

context: The Sun–Earth system. If position is measured from the Moon and if we start by supposing that x, $y \ll z \ll 1$, the equations of motion are (approximately):

$$\ddot{x} - 2\dot{y} \cong 3x + \tfrac{3}{2}z^2 - \frac{\mu x}{z^3}$$

$$\ddot{y} + 2\dot{x} \cong -\frac{\mu y}{z^3} \tag{4.1}$$

$$\ddot{z} \cong -z - \frac{\mu}{z^2}$$

in which the only important second-order term in the expansion of $\nabla(1/d_\oplus)$ about the Moon is the term $\tfrac{3}{2}z^2$ in the x-component.

The third equation, $(4.1)_3$, leads to an obvious integral:

$$\frac{\dot{z}^2}{2} + \frac{1}{2}z^2 - \frac{\mu}{z} = \mathscr{E}, \qquad \text{a constant.} \tag{4.2}$$

We may introduce the dimensionless parameter $\eta\,(-\infty < \eta < 1)$ related to $\mathscr{E}$ and $z_{\max}$ by:

$$\eta = \frac{2\mathscr{E}}{z_{\max}^2} = 1 - \frac{2\mu}{z_{\max}^3}, \tag{4.3}$$

and related in turn to the Jacobi constant C by:

$$C = 3 - 4\mu + \mu^2 - \eta\left(\frac{2\mu}{1-\eta}\right)^{2/3} \tag{4.4}$$

Equation (4.2) leads to a quadrature for the time from $z = 0$,

$$t = \int\limits_0^{z/z_{max}} \frac{\sqrt{\zeta}\,d\zeta}{\sqrt{(1-\zeta)(1-\eta+\zeta+\zeta^2)}}, \tag{4.5}$$

which is an elliptic integral of the third kind.

The relatively small deviations x, y from the z-axis satisfy the first two equations (4.1)$_1$ and (4.1)$_2$, which are non-homogeneous linear with time-varying coefficients and forcing term. The assumption $x, y \ll z$ eliminates, of course, the brief period of time when the orbit is closest to the Moon and when the Earth's effect on the orbit is small. If the variables x, y, $\dot{x}$, $\dot{y}$, are replaced by certain osculating Moon-centered orbit elements, the resulting differential equations will be valid throughout the orbit. Specifically we chose,

$$P_1 = \left(\frac{1-\eta}{2}\right)^{1/3} \frac{y\dot{z}-z\dot{y}}{z_{max}^2\left(\frac{1-\eta}{2}+\zeta^3\right)}, \qquad P_3 = \left(\frac{1-\eta}{2}\right)^{1/3} \frac{x\dot{z}-\dot{z}x}{z_{max}^2\left(\frac{1-\eta}{2}+\zeta^3\right)},$$

$$P_2 = \frac{(\dot{z}^2+z\ddot{z})y - z\dot{z}\dot{y}}{z^2\ddot{z}}, \qquad P_4 = \frac{(\dot{z}^2+z\ddot{z})x - z\dot{z}\dot{x}}{z^2\ddot{z}} \tag{4.6}$$

ζ denotes z/z_{max}; P_1, P_3 are proportional to the orbital angular momentum $\mathbf{r} \times \mathbf{v}$ (in the rotating frame); while P_2, P_4 are the small angular deviations from the z-axis of the apolune direction; i.e., P_2, P_4 are certain linear combinations [3] of $\pi/2 - i$ and $3\pi/2 - \omega$ where i, ω are the usual orbital elements, referred to the xy plane. The P's satisfy the linear non-homogeneous equation:

$$\frac{d}{ds}\begin{pmatrix} P_1 \\ P_2 \\ P_3 \\ P_4 \end{pmatrix} = \frac{4}{1-\eta+2\zeta^3} \begin{pmatrix} \sqrt{\zeta} & 0 \\ sR/\xi & 0 \\ 0 & \sqrt{\zeta} \\ 0 & sR/\xi \end{pmatrix} \times$$

$$\times \left\{ \begin{pmatrix} 4s\zeta^{3/2} & -\zeta^2\xi/R & W/R & -2\xi s\sqrt{\zeta} \\ -W/R & 2\xi s\sqrt{\zeta} & 7s\zeta^{3/2} & -4\zeta^2\xi/R \end{pmatrix} \begin{pmatrix} P_1 \\ P_2 \\ P_3 \\ P_4 \end{pmatrix} - \frac{\frac{3}{2}\mu^{1/3}\zeta^3}{R}\begin{pmatrix} 0 \\ 1 \end{pmatrix} \right\} \tag{4.7}$$

where R denotes $\sqrt{1-\eta+\zeta+\zeta^2}$, W denotes $1-\eta+2\eta\zeta-4\zeta^3$, ξ denotes $[(1-\eta)/2]^{1/3}$ and where the independent variable s is defined by:

$$s = \begin{cases} -\sqrt{1-\zeta}, & \dot{z} > 0, \\ +\sqrt{1-\zeta}, & \dot{z} < 0. \end{cases} \tag{4.8}$$

This independent variable has several advantages; in the first place it is not necessary to invert (4.5) and express ζ as a function of t, and the infinite value of $\dot{z}$ at $z = 0$ is not a problem; secondly, the vanishing of $\dot{z}$ at $z = z_{max}(\zeta = 1)$ makes s preferable to z or ζ.

The linearity of Equation (4.7) leads to a simple form for the P's at $s = +1$ (return) in terms of the P's at $s = -1$ (departure):

$$\begin{pmatrix} P_1(+1) \\ P_2(+1) \\ P_3(+1) \\ P_4(+1) \end{pmatrix} = T(\eta) \begin{pmatrix} P_1(-1) \\ P_2(-1) \\ P_3(-1) \\ P_4(-1) \end{pmatrix} + \mu^{1/3} A(\eta), \tag{4.9}$$

where $T(\eta)$ is the solution (at $s = 1$) of the homogeneous matrix equation associated with (4.7), the initial matrix being the identity (at $s = -1$), and $\mu^{1/3} A(\eta)$ is the solution of (4.7) with the zero initial P's $(P_i(-1) = 0)$.

The desired periodic orbits are given by:

$$[\vartheta_4 - T(\eta)] \begin{pmatrix} P_1(-1) \\ P_2(-1) \\ P_3(-1) \\ P_4(-1) \end{pmatrix} = \mu^{1/3} A(\eta), \tag{4.10}$$

where ϑ_4 denotes the 4×4 identity matrix, and they are unstable if the eigen-values of $T(\eta)$ lie outside the unit-circle. These periodic orbits have been computed for various η; in every case $P_2(-1)$ and $P_3(-1)$ are zero, indicating perpendicular crossing of the xz plane. The eigen-values of $T(\eta)$, moreover, are in quite good agreement, at least if $\eta < -3.5$ ($z_{max} < 68\ 000$ km), with the eigen-values of M associated with the exact, numerically integrated, orbits. The agreement of the orbit $x(z)$, $y(z)$ is moderately good and improves, as expected, when z_{max} decreases, as is evident in Figure 5, where z_{max} is plotted vs x_{max}. The stability of the periodic solutions of (4.7) changes with increasing η at $\eta = -3.543$ ($z_{max} = 67\ 300$ km) when one pair of eigen-values of $T(\eta)$ leaves the unit-circle at -1. At $\eta = -2.471$ ($z_{max} = 73\ 600$ km), moreover, the other pair of eigen-values leaves the unit-circle at $+1$. The periodic solution, given by (4.10) leads to infinitely large positive x as $\eta \to -2.471$ from below (see Figure 5).

5. A Second Halo Family Emanating from Near L_1

For $\eta > -2.471$, the solution of (4.10) reappears from infinity with opposite sign. It was therefore conjectured that the corresponding $x(z)$, $y(z)$ approximate a portion of a second family of halo periodic orbits, in this case emanating from the vicinity of L_1. This conjecture has been verified and the values $|x_{max}|$, z_{max} are shown for both families in Figure 5, together with the approximations (dotted lines) furnished by the almost rectilinear theory.
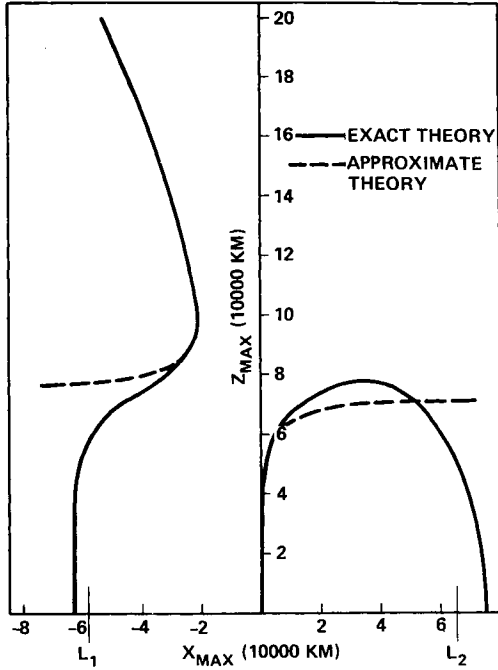
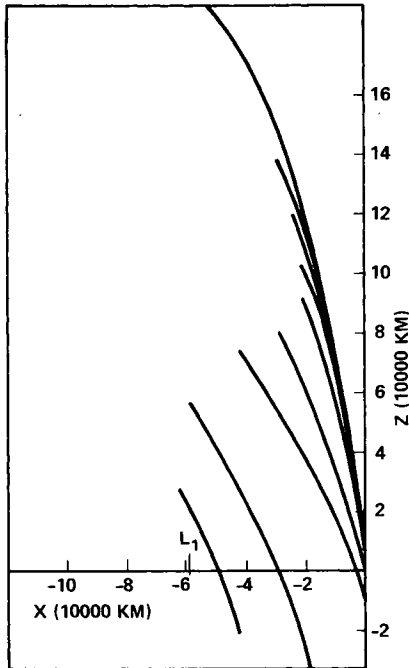Fig. 5.   The Halo family apolune points.

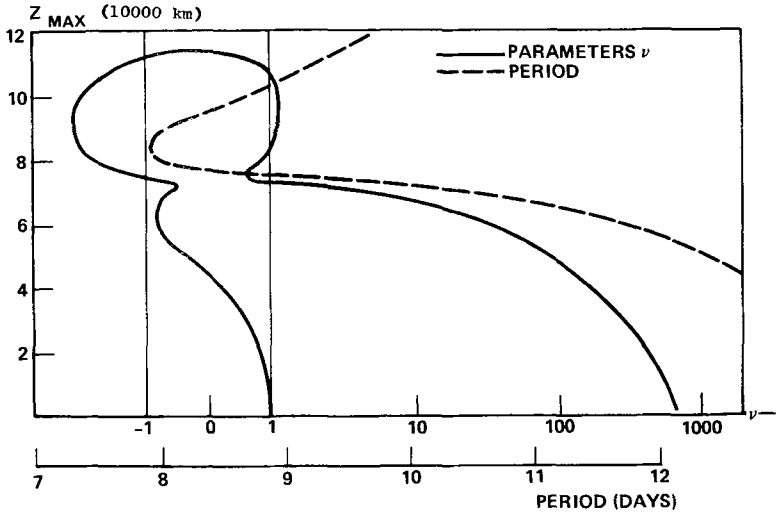Fig. 6. X–Z projection of the L_1 halo family.

Fig. 7.   Stability parameters ν_i and period (L_1 branch).

The xz projections of the new family are shown in Figure 6, and the values of the stability indices ν_1, ν_2 are plotted vs z_{max}, along with the period in Figure 7 up to $z_{max} = 113\ 000$ km. Again there is a narrow band of stable orbits, for $73\ 000$ km $<$ $z_{max} < 74\ 500$ km, shown in projections in Figures 8. The angular momentum vector $\mathbf{h}/\mathbb{C}$ and the torque due to the Earth's gravity gradient are opposite to those for the L_2 family, again causing the orbit to precess and remain fixed in the rotating frame. As
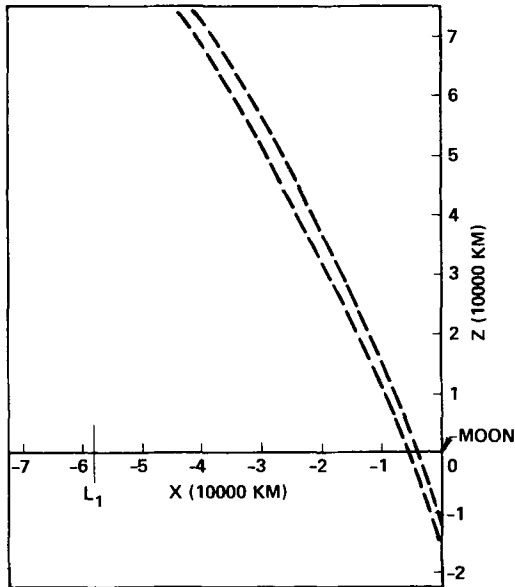

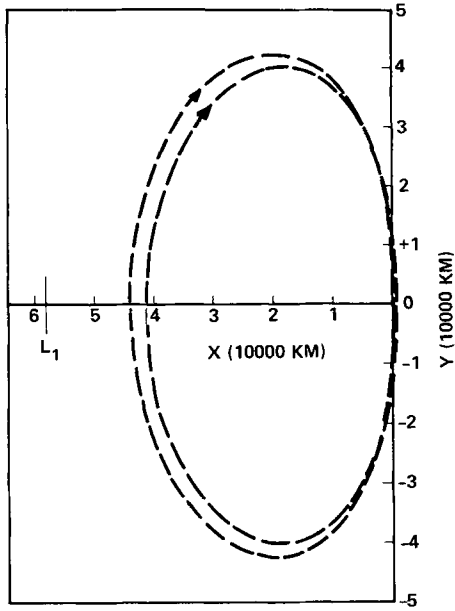Fig. 8a.   Stable orbit X–Z position bounds, L_1 branch.

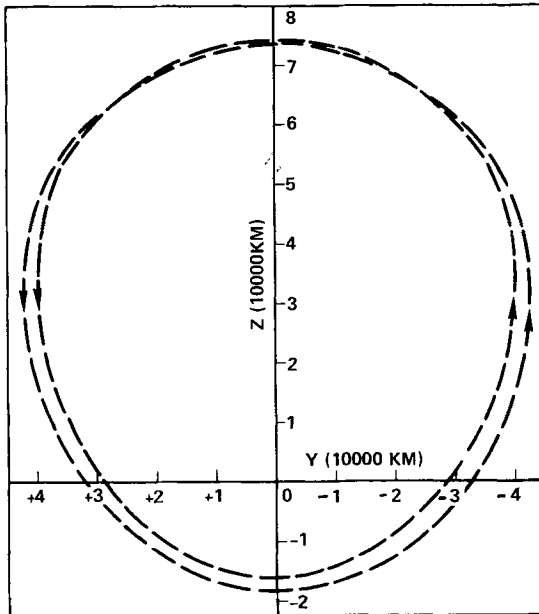Fig. 8b.   Stable orbit X–Y position bounds, L_2 branch.

Fig. 8c.   Stable orbit Y–Z position bounds, L_1 branch.

z_{max} increases further we encounter a second narrow band of stable orbits, for $112\,000\text{ km} < z_{max} < 113\,000\text{ km}$. This band has perilune below the lunar surface. At $z_{max} = 113\,000$ km the two ν_i's coincide, and for larger z_{max} we obtain instability due to a pair of complex conjugate eigen-values λ outside the unit-circle, their reciprocals lying inside the unit-circle. Figure 9 shows the behavior of those λ's having positive imaginary part as z_{max} increases beyond $113\,000$ km. The perilune distance, meanwhile, continues to decrease until z_{max} reaches $130\,000$ km.
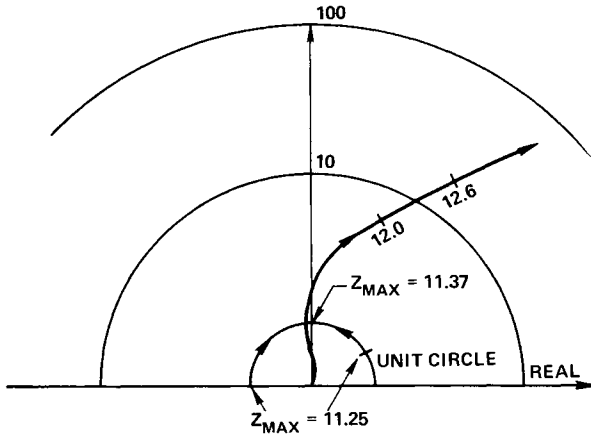

Fig. 9. Eigenvalues for higher z_{max}.

6. Conclusions and Recommendations

The Halo orbits originating in the vicinities of both L_1 and L_2 grow larger, but shorter in period, as they shift towards the moon. There is in each case a narrow band of stable orbits roughly half-way to the Moon. Nearer to the Moon, the orbits are fairly well-approximated by an 'almost rectilinear' analysis described in [3]. The L_2 family shrinks in size as it approaches the Moon, becoming stable again shortly before penetrating the lunar surface. The L_1-family becomes longer and thinner as it approaches the Moon, with a second narrow band of stable orbits with perilune, however, below the lunar surface.

It would be interesting to pursue the L_1-family for even greater z_{max}. It would also be interesting to examine the neighborhoods of that member of the L_2 family, and of the two members of the L_1 family, where one $\nu_i = +1$ and the Jacobi constant has an extreme value, to see if there are any bifurcations onto new branches of periodic orbit families.

The stable bands, roughly half-way from the Moon to L_1 and L_2, are of special possible significance in view of recent interest in a space colony built of lunar material [4]. It is desirable to investigate the influence on their stability of both lunar orbit eccentricity and solar gravity.

References

1. Farquhar, R. W. and Kamel, A. A.: 1973, 'Quasi-Periodic Orbits About the Translunar Libration Point', *Celest. Mech.* **7**, 458.
2. Farquhar, R. W.: 1970, 'The Control and Use of Libration-Point Satellites', NASA TR R-346.
3. Breakwell, J. V.: 1973, 'Trajectories Launched Normal to the Elliptic', Proc. of the XIV International Astronautical Congress, Paris.
4. O'Neill, G. K.: 1974, 'The Colonization of Space', *Physics Today*.